Antagonistic control of active surface integrins by myotubularin and phosphatidylinositol 3-kinase C2β in a myotubular myopathy model

Paula Samsó, Philipp A. Koch, York Posor, Wen-Ting Lo, Hassane Belabed, Marc Nazare, Jocelyn Laporte, Volker Haucke

PNAS RESEARCH ARTICLE | CELL BIOLOGY

Antagonistic control of active surface integrins by myotubularin and phosphatidylinositol 3-kinase C2β in a myotubular myopathy model

Paula Samsó[a,1], Philipp A. Koch[a,1], York Posor[a], Wen-Ting Lo[a], Hassane Belabed[b], Marc Nazare[b], Jocelyn Laporte[c], and Volker Haucke[a,d,2]

Edited by Pietro De Camilli, Yale University, New Haven, CT; received February 9, 2022; accepted August 29, 2022

X-linked centronuclear myopathy (XLCNM) is a severe human disease without existing therapies caused by mutations in the phosphoinositide 3-phosphatase MTM1. Loss of MTM1 function is associated with muscle fiber defects characterized by impaired localization of β-integrins and other components of focal adhesions. Here we show that defective focal adhesions and reduced active β-integrin surface levels in a cellular model of XLCNM are rescued by loss of phosphatidylinositiol 3-kinase C2β (PI3KC2β) function. Inactivation of the *Mtm1* gene impaired myoblast differentiation into myotubes and resulted in reduced surface levels of active β1-integrins as well as corresponding defects in focal adhesions. These phenotypes were rescued by concomitant genetic loss of *Pik3c2b* or pharmacological inhibition of PI3KC2β activity. We further demonstrate that a hitherto unknown role of PI3KC2β in the endocytic trafficking of active β1-integrins rather than rescue of phosphatidylinositol 3-phosphate levels underlies the ability of *Pik3c2b* to act as a genetic modifier of cellular XLCNM phenotypes. Our findings reveal a crucial antagonistic function of MTM1 and PI3KC2β in the control of active β-integrin surface levels, thereby providing a molecular mechanism for the adhesion and myofiber defects observed in XLCNM. They further suggest specific pharmacological inhibition of PI3KC2β catalysis as a viable treatment option for XLCNM patients.

myotubular myopathy | integrins | focal adhesions | phosphoinositides | endocytosis

Significance

X-linked centronuclear myopathy (XLCNM) is a severe human disease characterized by muscle fiber defects that result from mutations in the gene encoding the lipid phosphatase MTM1. At present there are no approved therapies for XLCNM. We show that loss of the lipid kinase PI3KC2β restores normal cell-surface levels of active β-integrin adhesion receptors in a cellular model of XLCNM via a mechanism that involves endocytic trafficking of active β1-integrins rather than rescue of signaling lipid levels. Specific pharmacological inhibition of PI3KC2β activity may thus be a viable treatment option for XLCNM patients.

X-linked centronuclear myopathy (XLCNM) is a severe congenital myopathy characterized by muscle weakness and disorganization, among other muscle and nonmuscle symptoms. About one-third of affected boys die in the first year of life, and the surviving children suffer from significant morbidities, including chronic ventilator and wheelchair dependence, resulting in a dramatically reduced lifespan. Muscle biopsies from XLCNM patients display a severe variation in fiber size due to the presence of small, round fibers with centrally placed nuclei as well as abnormalities of the muscle triad (1). Currently, no approved specific therapy is available for XLCNM patients. XLCNM is caused by loss-of-function mutations in the phosphoinositide 3-phosphatase MTM1 (1, 2), a major regulator of the endosomal signaling lipids phosphatidylinositol-3-phosphate [PI(3)P] and phosphatidylinositol-3,5-bisphosphate [PI(3,5)P_2] (3–8). Loss or depletion of MTM1 in mice, *Drosophila melanogaster*, or XLCNM patient-derived fibroblasts causes the intracellular accumulation of the key focal adhesion (FA) components β1-integrins within the endosomal system (5, 9, 10). Integrin localization defects were also found in human XLCNM muscle fibers (10). β1-integrins are essential for differentiation, maintenance, and regeneration of skeletal muscle due to their roles in myotube fusion, muscle-specific adhesion and contractile machinery, signaling, and stem cell renewal (10–13). Hence, one might hypothesize that the structural and functional muscle fiber defects in animal models and XLCNM patients are due to defective β1-integrin localization caused by loss of MTM1 function. In support of this hypothesis, it has been observed that MTM1-mediated hydrolysis of endosomal PI(3)P controls the exocytic delivery of membrane proteins including β1-integrins in nonmuscle cells (5) as well as *D. melanogaster* muscle (10).

Genetic studies in *D. melanogaster*, zebrafish, and mice suggest that the phenotypic symptoms of XLCNM can be rescued by muscle-specific deletion of *Pik3c2b* (14, 15), a ubiquitously expressed class II phosphatidylinositol 3-kinase (PI3K). PI3KC2β has been shown to synthesize PI(3)P or phosphatidylinositol 3,4-bisphosphate [PI(3,4)P_2] (i.e., a non-MTM1 substrate lipid), possibly in a cell-type and/or subcellular location-specific (e.g., endosomes, lysosomes, and plasma membrane) manner to regulate a variety of processes including insulin signaling, nutrient signaling via mTORC1, and cell migration (16–21). It has, thus, been hypothesized that the reversal of the XLCNM disease process

Author affiliations: [a]Department of Molecular Pharmacology & Cell Biology, Leibniz-Forschungsinstitut für Molekulare Pharmakologie, 13125 Berlin, Germany; [b]Medicinal Chemistry, Leibniz-Forschungsinstitut für Molekulare Pharmakologie, 13125 Berlin, Germany; [c]Department of Translational Medicine and Neurogenetics, Institut de Génétique et de Biologie Moléculaire et Cellulaire, INSERM U1258, CNRS UMR7104, Strasbourg University, 67404 Illkirch, France; and [d]Faculty of Biology, Chemistry and Pharmacy, Freie Universität Berlin, 14195 Berlin, Germany

Author contributions: P.S., P.A.K., H.B., M.N., J.L., and V.H. designed research; P.S., P.A.K., Y.P., W.-T.L., and H.B. performed research; H.B. and M.N. contributed new reagents/analytic tools; P.S., P.A.K., Y.P., W.-T.L., H.B., and V.H. analyzed data; M.N. and V.H. wrote the paper; and V.H. supervised the project.

The authors declare no competing interest.

This article is a PNAS Direct Submission.

[1]P.S. and P.A.K. contributed equally to this work.

[2]To whom correspondence may be addressed. Email: haucke@fmp-berlin.de.

This article contains supporting information online at http://www.pnas.org/lookup/suppl/doi:10.1073/pnas.2202236119/-/DCSupplemental.

Published September 26, 2022.

elicited by loss of PI3KC2β function involves its ability to synthesize 3-phosphoinositides, i.e., PI(3)P (15), as further indicated by the ability of the pan-PI3K inhibitor wortmannin to modestly improve motor function and prolong lifespan of MTM1 knockout (KO) mice (14). Whether and how PI3KC2β exhibits a specific role in muscle cells, in particular with respect to β1-integrins, and how its function may relate to XLCNM at the molecular mechanistic level are unknown.

Here we unravel a crucial antagonistic function of MTM1 and PI3KC2β in the cell-autonomous control of active β1-integrin surface levels, thereby providing a molecular mechanism for the adhesion and myofiber defects observed in XLCNM. Our findings further suggest that pharmacological blockade of PI3KC2β function by specific small-molecule inhibitors may serve as a potential treatment option for XLCNM in patients.

Results

Defective FAs and Reduced Active β1-Integrin Surface Levels in a Cell-Based Model of XLCNM. Previous studies have shown that loss of MTM1 in *D. melanogaster* or KO mice causes the intracellular retention of β1-integrins in endosomes in vivo (9, 10) and results in defects in myoblast fusion into myotubes (9, 22–24). Moreover, genetic studies suggest that the phenotypic symptoms of XLCNM in animal models can be rescued by deletion of the sole class II PI3K gene in *Drosophila* (15) or *Pik3c2b* in mice and zebrafish (14), possibly via a mechanism that involves restoration of PI(3)P levels (15). To obtain a better mechanistic understanding of the phenotypes elicited by MTM1 loss, in particular its role in myotube formation and integrin trafficking, we generated three independent C2C12 myoblast MTM1 KO lines via CRISPR-Cas9–mediated genome engineering. The disruption of the *Mtm1* locus was verified by genomic DNA sequencing (*Materials and Methods*) and lack of MTM1 protein expression was confirmed by immunoblotting (*SI Appendix*, Fig. S1*A*). Given the reported defects in muscle fiber size in MTM1 KO mice (9, 14, 25, 26), we assessed the ability of MTM1 KO myoblast C2C12 cells to fuse into multinucleated myotubes using myosin heavy chain (MHC) as a differentiation marker (*SI Appendix*, Fig. S1*B*). MTM1 KO led to a significant reduction in the average number of nuclei per MHC-positive myotube (referred to as differentiation index) and a greatly reduced fraction of multinucleated cells (i.e., 6 to 15 or >15 nuclei per myotube) compared to wild-type (WT) C2C12 (Fig. 1 *A* and *B*). More variable differences were observed in the nuclear fusion index (i.e., the fraction of nuclei within MHC-positive myotubes) in our MTM1 KO C2C12 clones (*SI Appendix*, Fig. S1*C*). These corresponded with a reduced expression of MHC and myogenin in the MTM1 KO clone 1 but not in clones 2 and 3 (*SI Appendix*, Fig. S1*D*). These data suggest that loss of MTM1 results in defective myotube formation, in agreement with other models and previous reports (9, 22–24).

As β-integrins (11, 12) and FAs (27) are important for myoblast fusion and myofiber assembly, we hypothesized that the observed defect in myotube formation of MTM1 KO myoblasts may originate from defective FA assembly as a consequence of alterations in integrin localization due to loss of MTM1. To test this hypothesis we analyzed cell spreading, FA number, and β1-integrin localization in undifferentiated C2C12 myoblasts. Undifferentiated MTM1 KO myoblasts displayed a reduced cell area-to-volume ratio (Fig. 1*C*) as a result of impaired cell spreading (*SI Appendix*, Fig. S1*E*), whereas the total cell volume (i.e., cell size) was unaltered (*SI Appendix*, Fig. S1*F*). Cell spreading and FA dynamics largely depend on the function of plasma membrane-localized active β-integrins (27). MTM1 KO C2C12 myoblasts displayed a significant reduction in the number of FAs marked by paxillin (Fig. 1 *D* and *E*). A similar reduction was observed for other FA markers such as vinculin and zyxin (*SI Appendix*, Fig. S1 *G–I*). We then probed the surface levels and localization of active β1-integrins using well-established conformation-specific antibodies (28–31). The surface levels of active β1-integrins (Fig. 1 *F* and *G*), but not those of total β1-integrins (*SI Appendix*, Fig. S1*J*), were greatly reduced in MTM1 KO C2C12 myoblasts. Analysis of total surface β1-integrin levels by fluorescence-activated cell sorting (FACS) confirmed the reduction of cell surface active β1-integrins upon loss of MTM1 (*SI Appendix*, Fig. S1*K*). Total β1-integrins appeared to be slightly increased upon MTM1 loss when analyzed by FACS (*SI Appendix*, Fig. S1*L*). Consistent with the reduced levels of active β1-integrins, MTM1 KO myoblasts displayed reduced pFAK (*SI Appendix*, Fig. S2 *A* and *B*) and pAKT1 (*SI Appendix*, Fig. S2 *C* and *D*) levels, established downstream effectors of integrin signaling. To explore whether the role of MTM1 in FA assembly and β1-integrin surface delivery depends on its 3-phosphatase activity, we conducted rescue experiments in MTM1 KO myoblasts. Reexpression of WT but not catalytically inactive (C375S) MTM1 potently promoted β1-integrin delivery to the cell surface (*SI Appendix*, Fig. S2 *E* and *F*). This correlated with the restoration of normal PI(3)P levels by WT but not by inactive MTM1 (*SI Appendix*, Fig. S2 *E* and *G*).

FAs serve as anchoring points for cells in tissues including muscle and, thereby, limit the speed of migration (27). Consistent with the observed reduction in FA number MTM1 KO myoblasts displayed increased speed of migration (*SI Appendix*, Fig. S2*H*). MTM1 KO C2C12 myoblasts also recapitulated other reported features of XLCNM models including defective organization of desmin intermediary filaments and dispersion of transferrin receptor-containing recycling endosomes (5) to the cell periphery (*SI Appendix*, Fig. S2 *I* and *J*).

Collectively, these data indicate that MTM1 KO myoblasts recapitulate key features of XLCNM in animal models and in humans, most notably a cell-autonomous defect in surface delivery of active β1-integrins resulting in reduced numbers of FAs as a result of defective PI 3-phosphate hydrolysis.

Genetic Loss of PI3KC2β Rescues Defective Myotube Differentiation and Restores Normal Active β1-Integrin Surface Levels. As genetic studies suggest that *Pik3c2b* acts as a genetic modifier of XLCNM pathology in vivo (14), we decided to explore the potential role of PI3KC2β in myoblasts and in the modulation of XLCNM at the molecular mechanistic level by creating MTM1/PI3KC2β double-KO C2C12 cells (Fig. 2 and *SI Appendix*, Fig. S3). Immunoblot analysis of MTM1 KO myoblasts showed that loss of MTM1 is associated with reduced steady-state levels of PI3KC2β protein, as often seen for proteins that act together in a common genetic pathway. Neither MTM1 nor PI3KC2β were detectable in a double-KO myoblast line generated by CRISPR-Cas9 (double KO#1) (*SI Appendix*, Fig. S3*A*). We then analyzed the ability of WT or KO myoblasts lacking either MTM1, PI3KC2β, or both proteins to differentiate into multinucleated MHC-positive myotubes (Fig. 2 *A–D*). In contrast to the defects in myotube differentiation observed in MTM1 KO myoblasts (Fig. 1), MTM1/PI3KC2β double-KO myoblasts were indistinguishable from WT cells with respect to myotube differentiation as evidenced by a normal differentiation index (Fig. 2*B*), nuclear fusion index (Fig. 2*C*), and the fraction of multinucleated cells (Fig. 2*D*). MTM1/PI3KC2β double-KO myoblasts also showed normal levels of myogenin and MHC expression

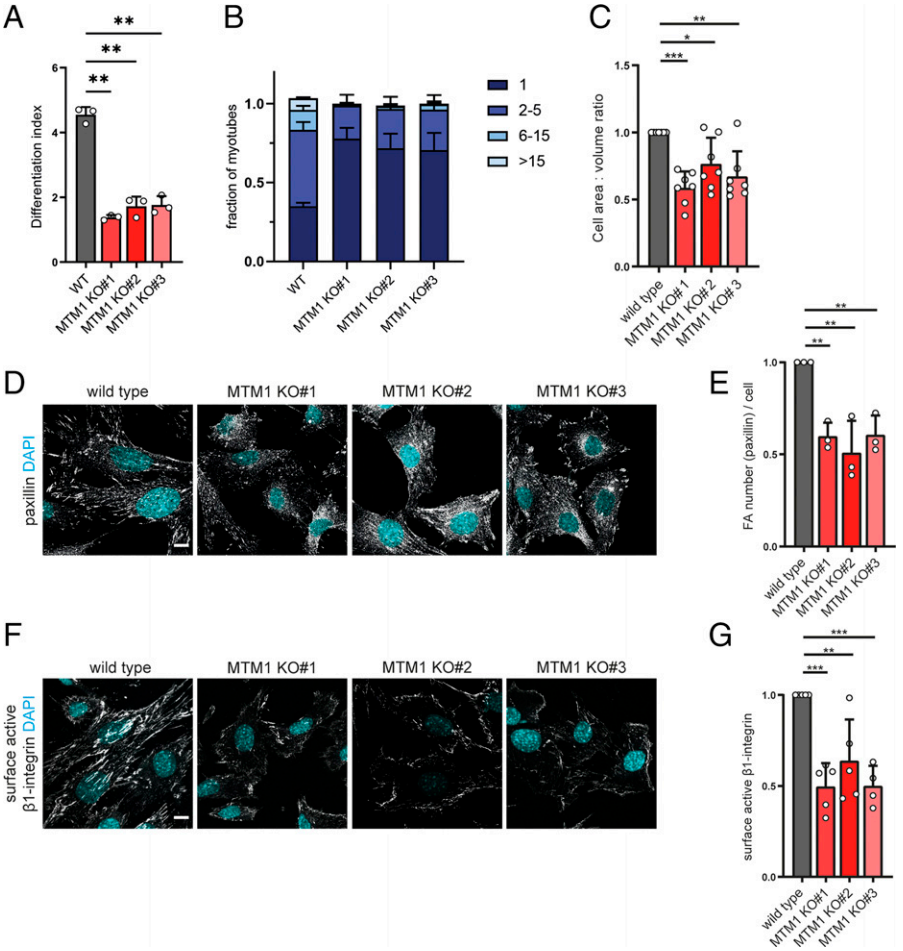

Fig. 1. Defective differentiation, FAs, and reduced active β1-integrin surface levels in a cell-based model of XLCNM. (*A*) Differentiation index (number of nuclei/MHC-positive myotube) of WT and MTM1 KO C2C12 cells differentiated for 6 d. Mean ± SD from three independent experiments compared to WT. For each experiment, 10 images (850 μM × 850 μM) were acquired per condition. One-way ANOVA ($F = 32.71$) and Tukey's multiple-comparison test; $^{**}P < 0.01$. WT vs. MTM1 KO#1 $P = 0.0032$; WT vs. MTM1 KO#2 $P = 0.0077$; WT vs. MTM1 KO#3 $P = 0.0085$. (*B*) Fraction of myotubes containing 1, 2 to 5, 6 to 15, or >15 nuclei of WT and MTM1 KO C2C12 cells differentiated for 6 d. Mean ± SD from three independent experiments. For each experiment, 10 images (850 μm × 850 μm) were acquired per condition. Two-way RM ANOVA and Dunnett's multiple comparison test; 1 nucleus: WT vs. MTM1 KO#1 $^{**}P = 0.0097$; WT vs. MTM1 KO#2 $^{*}P = 0.0305$; WT vs. MTM1 KO#3 $^{*}P = 0.0486$; 2 to 5 nuclei: WT vs. MTM1 KO#1 $^{*}P = 0.0147$; WT vs. MTM1 KO#2 $^{*}P = 0.0347$: WT vs. MTM1 KO#3 ns $P = 0.0652$; 6 to 15 nuclei: WT vs. MTM1 KO#1 $^{*}P = 0.260$; WT vs. MTM1 KO#2 $^{*}P = 0.0180$: WT vs. MTM1 KO#3 $^{*}P = 0.0220$; >15 nuclei: WT vs. MTM1 KO#1 $^{**}P = 0.0058$; WT vs. MTM1 KO#2 $^{***}P = 0.0005$: WT vs. MTM1 KO#3 $^{**}P = 0.0013$. (*C*) Relative cell area to volume ratio of WT and MTM1 KO C2C12 undifferentiated myoblasts measured by FACS. Mean ± SD from seven independent experiments represented as fold change compared to control (WT) with a hypothetical mean of 1. Cell areas were determined from 10 images per condition per experiment accounting for 50 to 100 cells. Forward scatter values were obtained from 10,000 cells per experiment per condition. One-way ANOVA ($F = 9.795$) and Dunnett's multiple-comparison test; WT vs. MTM1 KO#1 $^{***}P = 0.0001$, WT vs. MTM1 KO#2 ns $P = 0.1342$, WT vs. MTM1 KO#3 $^{**}P = 0.0016$. (*D*) Representative images of WT and MTM1 KO C2C12 undifferentiated myoblasts immunostained for active paxillin and DAPI for nuclear staining. (Scale bar, 10 μm.) (*E*) Number of FAs per cell in WT and MTM1 KO C2C12 undifferentiated myoblasts measured using paxillin as FA marker. Mean ± SD from three independent experiments represented as fold change compared to control (WT) with a hypothetical mean of 1. 10 images per condition and experiment were acquired accounting for 50 to 100 cells. One-way ANOVA ($F = 12.33$) and Dunnett's multiple-comparison test; WT vs. MTM1 KO#1 $^{**}P = 0.0048$, WT vs. MTM1 KO#2 $^{**}P = 0.0014$, WT vs. MTM1 KO#3 $^{**}P = 0.0054$. (*F*) Representative images of WT and MTM1 KO C2C12 undifferentiated myoblasts immunostained under nonpermeabilizing conditions for active β1-integrin and DAPI for nuclear staining. (Scale bar, 10 μm.) (*G*) Surface active β1-integrin intensity per cell in WT and MTM1 KO C2C12 undifferentiated myoblasts measured by immunofluorescence. Mean ± SD from four or five independent experiments represented as fold change compared to control (WT) with a hypothetical mean of 1. 10 images per condition and experiment were acquired accounting for 50 to 100 cells on average. One-way ANOVA ($F = 13.12$) and Dunnett's multiple-comparison test; WT vs. MTM1 KO#1 $^{***}P = 0.0002$, WT vs. MTM1 KO#2 $^{**}P = 0.0033$, WT vs. MTM1 KO#3 $^{***}P = 0.0003$.

(*SI Appendix*, Fig. S1*D*). Normal myotube differentiation (Fig. 2 *B*–*D*) was also observed in a second genome-engineered myoblast cell line ($MTM1^{hypo}$/PI3KC2β KO) lacking detectable PI3KC2β protein expression and with severely reduced MTM1 protein content (*SI Appendix*, Fig. S3*B*). MTM1/PI3KC2β double-KO myoblasts also showed normal cell spreading (*SI Appendix*, Fig. S3*C*) and cell area-to-volume ratio (Fig. 2*E*). Moreover, the levels of active β1-integrins displayed on the double-KO cell surface (Fig. 2 *F* and *G*) as well as the number of zyxin-containing FAs (Fig. 2 *H* and *I*) were indistinguishable from WT cells, as was the speed of cell migration (Fig. 2*J*). Normal cell area, cell spreading, and levels of FA proteins (e.g., zyxin) as well as plasma membrane-localized active β1-integrins were also observed in PI3KC2β KO myoblasts (Fig. 2 *E*–*I*) and in the $MTM1^{hypo}$/PI3KC2β KO cell line (*SI Appendix*, Fig. S3 *D*–*I*). These results support the hypothesis that the observed rescue of XLCNM phenotypes in double-KO myoblasts is a specific phenotype due to functional genetic interactions between *Mtm1* and *Pik3c2b* rather than phenotypic differences originating from clonal selection. Consistently, elevated β1-integrin surface pools were also observed in MTM1 KO myoblasts subjected to short hairpin RNA–mediated knockdown of PI3KC2β expression (*SI Appendix*, Fig. S3*J*).

Our findings show that genetic loss of PI3KC2β rescues defective myotube differentiation, cell spreading, and FA number and

restores normal active β1-integrin surface levels induced by lack of functional MTM1 in myoblasts.

Rescue of β1-Integrin Surface Pools by Loss of Active PI3KC2β Neither Involves mTORC1 nor Restoration of Cellular PI(3)P Levels. The pathology of XLCNM as well as the cellular and organismal phenotypes of MTM1 loss of function are linked to its enzymatic activity as a 3-phosphatase that controls the levels of endosomal PI(3)P and, possibly, PI(3,5)P_2 (4, 7, 8, 15, 32, 33). While the reliable determination of PI(3,5)P_2 levels in cells remains difficult, endosomal PI(3)P can be detected and semi-quantitatively analyzed using the recombinant purified 2xFYVE domain of Hrs as a probe (34, 35). Consistent with prior studies (5, 15, 36), we found PI(3)P levels to be significantly elevated in three independent MTM1 KO myoblast cell lines compared to WT controls (*SI Appendix*, Fig. S4 *A* and *B*), while the total number over PI(3)P positive endosomes was not affected (*SI Appendix*, Fig. S4*C*). Furthermore, most detectable PI(3)P labeled by our approach resided on EEA1-positive endosomes (*SI Appendix*, Fig. S4 *D* and *E*). Conversely, PI3KC2β KO C2C12 cells displayed reduced levels of PI(3)P, suggesting that PI3KC2β contributes to PI(3)P synthesis in these cells [as in primary hepatocytes (17)], although it may not be the major source for endosomal PI(3)P (see below). Strikingly, MTM1/PI3KC2β double-KO myoblasts showed elevated PI(3)P levels similar to those observed in MTM1 single-KO cells (*SI Appendix*, Fig. S4 *F* and *G*). These data suggest that loss of *Pik3c2b* rescues cellular XLCNM phenotypes without restoring normal PI(3)P levels. We challenged these unexpected findings by exploring the effects of suppressing PI(3)P synthesis pharmacologically by application of a specific inhibitor of VPS34, the major contributor to endosomal PI(3)P synthesis in most cells and tissues (37, 38) including C2C12 myoblasts (*SI Appendix*, Fig. S4*H*). Prolonged inhibition of VPS34-mediated PI(3)P synthesis in the presence of VPS34-IN1 (39) failed to rescue the depletion of active β1-integrins from the surface of MTM1 KO myoblasts (Fig. 3*A* and *SI Appendix*, Fig. S4*I*), despite its ability to potently reduce endosomal PI(3)P levels. Hence, it appears that rescue of β1-integrin surface pools by loss of PI3KC2β is not mediated by restoration of endosomal PI(3)P levels.

Given these results and previous work showing that wortmannin, a broad-spectrum PI 3-kinase inhibitor targeting most PI 3-kinases including PI3KC2β, led to a mild rescue of muscle phenotypes in MTM1 KO mice (14), we considered alternative mechanisms. PI3KC2β in addition to its contribution to PI(3)P formation in some cell types (17, 18) has been shown to suppress mTORC1-mediated nutrient signaling via local synthesis of a lysosomal pool of phosphatidylinositol 3,4-bisphosphate [PI(3,4)P_2] in growth factor-deprived cells (19). Although PI(3,4)P_2 is not a substrate for MTM1 (40) and no consistent alterations in its levels were detected in the three KO myoblast lines, we considered the possibility that MTM1 and PI3KC2β might serve as antagonistic regulators of mTORC1 activity. However, we failed to detect changes in mTORC1 activity in MTM1 KO myoblasts assessed by the levels of its phosphorylated downstream substrate pS6K1 (Fig. 3*B*). Furthermore, prolonged application of different doses of the mTORC1 inhibitor rapamycin failed to restore normal levels of active β1-integrins on the surface of MTM1 KO myoblasts (Fig. 3*C* and *SI Appendix*, Fig. S4*J*). These data suggest that loss of *Pik3c2b* does not restore reduced surface levels of β-integrins caused by KO of MTM1 via elevation of mTORC1 signaling.

Our collective findings argue that the rescue of β1-integrin surface pools by loss of PI3KC2β in MTM1 KO cells either is 1) independent of its PI 3-kinase activity and/or 2) involves a mechanism that functions antagonistically to MTM1-mediated β1-integrin recycling to the cell surface (5, 10). To explore the putative function of PI3KC2β in integrin traffic more directly, we resorted to HeLa cells, which express much higher endogenous levels of PI3KC2β and less MTM1 compared to C2C12 myoblasts (Fig. 3*D*) and can be easily manipulated by RNA interference or plasmid-based expression. We used previously reported specific small interfering RNA (siRNA) to deplete HeLa cells of endogenous PI3KC2β (19) (*SI Appendix*, Fig. S4*K*) and monitored the levels of active β1-integrins on the cell surface. Loss of PI3KC2β led to pronouncedly elevated surface pools of active β1-integrins in HeLa cells (Fig. 3 *E* and *F*). This was paralleled by a moderate increase in the total β1-integrin levels in PI3KC2β-depleted cells (*SI Appendix*, Fig. S4*L*). Reexpression of siRNA-resistant WT but not kinase-inactive (KI) mutant PI3KC2β restored the surface pool of active β1-integrins to normal levels akin to those detected in control cells (Fig. 3 *E* and *F*).

These data together with the fact that loss of PI3KC2β does not appear to restore elevated PI(3)P levels in the absence of MTM1 expression (compare *SI Appendix*, Fig. S4 *C* and *D*) suggest that PI3KC2β may act on a different pool of 3-phosphoinositides, e.g., via synthesis of PI(3,4)P_2 (16, 19). To test this we capitalized on a class III-like mutant version of PI3KC2β, which is selectively defective in PI(3,4)P_2 synthesis but can generate PI(3)P with WT efficacy (16, 41). Strikingly, reexpression of mutant class III-like PI3KC2β failed to restore normal levels of β1-integrins in HeLa cells depleted of the endogenous enzyme (Fig. 3 *G* and *H*). These results indicate that the surface pool of active β1-integrins is controlled by PI3KC2β-mediated synthesis of PI(3,4)P_2 rather than PI(3)P.

PI3KC2β and MTM1 Antagonistically Control Active β1-Integrin Endocytosis and Recycling. Based on these findings and the known function of other class II PI3Ks in the endocytic pathway (18, 42), we hypothesized that PI3KC2β regulates the cell surface pools of active β-integrins by directly controlling their endocytosis and/or endosomal sorting (i.e., recycling vs. lysosomal degradation) (Fig. 4*A*) and, thereby, counteract MTM1-dependent β1-integrin delivery to the surface (5). We probed this hypothesis in multiple ways. As active β1-integrins are thought to be internalized at least in part via clathrin- and dynamin-dependent endocytosis (CME) (43), a process that depends on PI(3,4)P_2 (42), we depleted MTM1 KO myoblasts of either clathrin or dynamin 2. Inhibition of CME by knockdown of either clathrin or dynamin 2 rescued the levels of active β1-integrins on the cell surface of MTM1 KO myoblasts (Fig. 4*B*), consistent with the fact that reducing dynamin 2 expression rescues XLCNM in mice in vivo (44). To directly probe the putative function of PI3KC2β in the CME of β-integrins, we monitored its localization by total internal reflection fluorescence microscopy in genome-engineered HeLa cells endogenously expressing eGFP-PI3KC2β. We found eGFP-PI3KC2β to colocalize with endogenous clathrin-coated endocytic structures at the cell surface (*SI Appendix*, Fig. S5*A*). Further biochemical analysis revealed that endogenous eGFP-PI3KC2β associates with clathrin and other endocytic proteins including intersectin 1, a known binding partner of PI3KC2β (45) and the clathrin adaptor complex AP-2 (46), and with Dab2 (Fig. 4*C*), an endocytic adaptor for β-integrins (47). Affinity chromatography experiments paired with truncation

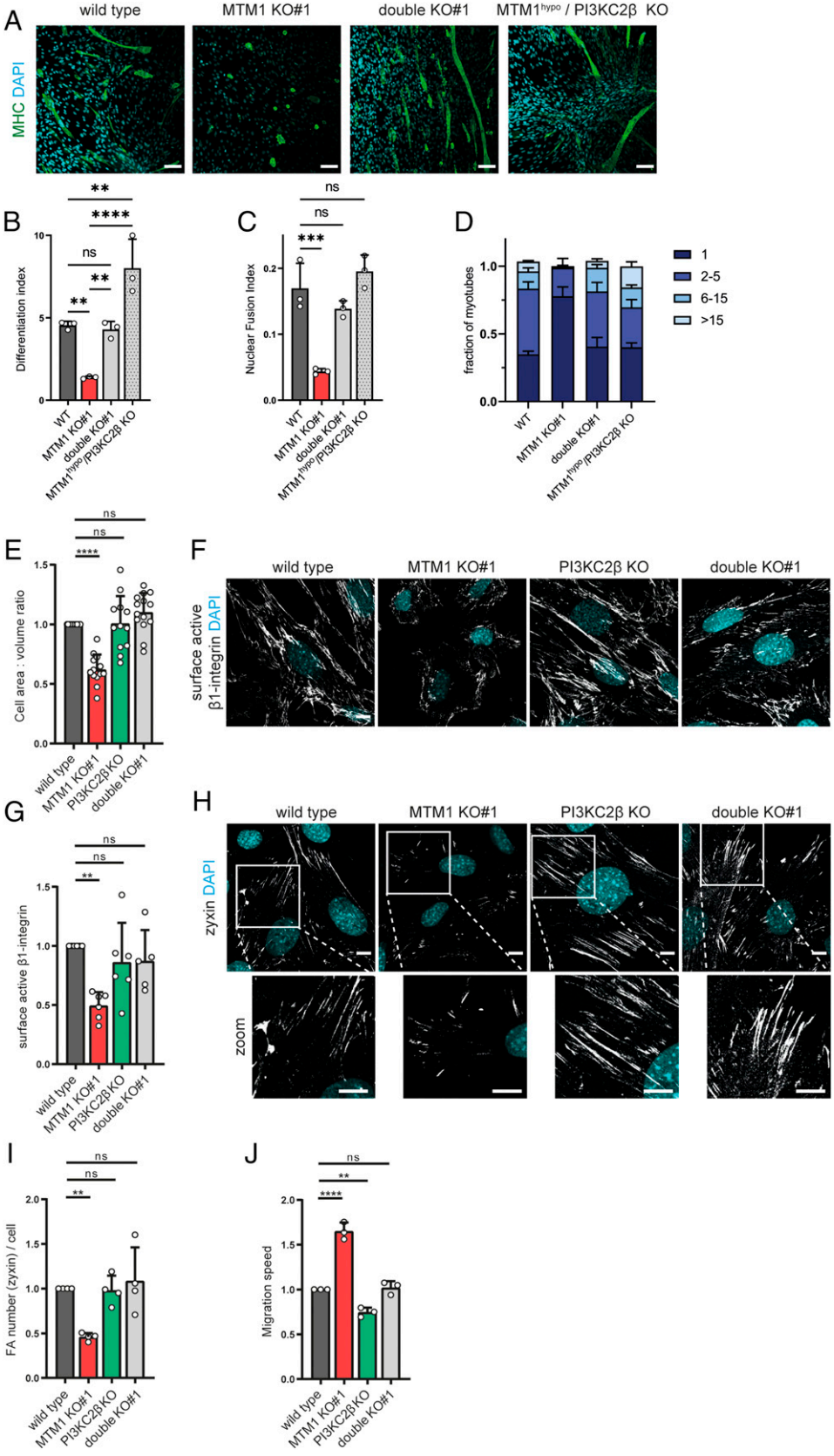

Fig. 2. Genetic loss of PI3KC2β rescues defective myotube differentiation and restores normal active β1-integrin surface levels. (*A*) Representative images of WT, MTM1 KO#1, double KO#1, and MTM1^{hypo}/PI3KC2β KO C2C12 myotubes differentiated for 6 d and immunostained for MHC as a differentiation marker and DAPI for nuclear staining. (Scale bar, 100 μm.) (*B*) Differentiation index (average number of nuclei per MHC positive myotube) of WT, MTM1 KO#1, double KO#1, and MTM1^{hypo}/PI3KC2β KO C2C12 myotubes differentiated for 6 d. Mean ± SD from three independent experiments compared to WT. Ten images (850 μM × 850 μM) per condition. One-way ANOVA ($F = 32.71$) and Tukey's multiple-comparison test; ns $P > 0.05$, *$P < 0.05$, **$P < 0.01$, ***$P < 0.001$, ****$P < 0.0001$. WT vs. MTM1 KO#1 $P = 0.0032$; WT vs. double KO#1 $P = 0.9980$; WT vs. MTM1$^{hypo/}$PI3KC2β KO $P = 0.0015$; MTM1 KO#1 vs. double KO#1 $P = 0.0061$; MTM1 KO#1 vs. MTM1$^{hypo/}$PI3KC2β KO $P < 0.0001$. (*C*) Nuclear fusion index (nuclei in myotubes per total number of nuclei) of WT, MTM1 KO#1, double KO#1, and MTM1^{hypo}/PI3KC2β KO C2C12 myotubes differentiated for 6 d. Mean ± SD from three independent experiments compared to WT. Ten images (850 μM × 850 μM) per condition. One-way ANOVA ($F = 15.96$) and Tukey's multiple-comparison test; ns $P > 0.05$, ***$P < 0.001$. WT vs. MTM1 KO#1 $P = 0.0003$; WT vs. double KO#1 $P = 0.6060$; WT vs. MTM1$^{hypo/}$PI3KC2β KO $P = 0.7549$. (*D*) Fraction of myotubes containing 1, 2 to 5, 6 to 15, or >15 nuclei of WT, MTM1 KO#1, double KO#1, and MTM1^{hypo}/PI3KC2β KO C2C12 myotubes differentiated for 6 d. Two-way RM ANOVA and Dunnett's multiple comparison test; 1 nucleus: WT vs. MTM1 KO#1 **$P = 0.0097$; WT vs. double KO#1 ns $P = 0.4915$; WT vs. MTM1$^{hypo/}$PI3KC2β KO ns $P = 0.1845$; 2 to 5 nuclei: WT vs. MTM1 KO#1 *$P = 0.0147$; WT vs. double KO#1 ns $P = 0.3660$; WT vs. MTM1$^{hypo/}$PI3KC2β KO *$P = 0.0284$; 6 to 15 nuclei: WT vs. MTM1 KO#1 *$P = 0.0260$; WT vs. double KO#1 ns $P = 0.1741$; WT vs. MTM1$^{hypo/}$PI3KC2β KO ns $P = 0.6133$; >15 nuclei: WT vs. MTM1 KO#1 **$P = 0.0058$; WT vs. double KO#1 ns $P = 0.2142$; WT vs. MTM1$^{hypo/}$PI3KC2β KO ns $P = 0.0936$. (*E*) Cell area of WT and C2C12 KO myoblasts. Mean ± SD from 13 to 16 independent experiments represented as fold change compared to control (WT) with a hypothetical mean of 1. One-way ANOVA ($F = 44.72$) and Dunnett's multiple-comparison test; WT vs. MTM1 KO#1 ****$P < 0.0001$, WT vs. PI3KC2β KO ns $P = 0.9712$, WT vs. double KO#1 ***$P = 0.0007$. (*F*) Representative images of WT, MTM1 KO#1, PI3KC2β KO#1, and double KO#1 undifferentiated myoblasts immunostained under nonpermeabilizing conditions for active β1-integrin and DAPI for nuclear staining. (Scale bar, 10 μm.) (*G*) Surface active β1-integrin intensity per cell in WT, MTM1 KO#1, PI3KC2β KO#1, and double KO#1 undifferentiated myoblasts. Mean ± SD from five or six independent experiments represented as fold change compared to control (WT) with a hypothetical mean of 1. Ten images per condition and experiment were acquired accounting for 50 to 100 cells. One-way ANOVA ($F = 6.0$) and Dunnett's multiple-comparison test; WT vs. MTM 1KO#1 **$P = 0.0020$, WT vs. PI3KC2β KO ns $P = 0.5683$, WT vs. double KO#1 ns $P = 0.6538$. (*H*) Representative images of WT, MTM1 KO#1, PI3KC2β KO#1, and double KO#1 undifferentiated myoblasts immunostained for zyxin and DAPI for nuclear staining. (Scale bar, 10 μm.) (*I*) Number of FAs per cell in WT, MTM1 KO#1, PI3KC2β KO#1, and double KO#1 undifferentiated myoblasts measured using zyxin as FA marker. Mean ± SD from four independent experiments represented as fold change compared to control (WT) with a hypothetical mean of 1. Ten images per condition and experiment were acquired accounting for 50 to 100 cells. One-way ANOVA ($F = 7.655$) and Dunnett's multiple-comparison test; WT vs. MTM1 KO#1 **$P = 0.0079$, WT vs. PI3KC2β KO ns $P = 0.9980$, WT vs. double KO#1 ns $P = 0.8806$. (*J*) Random migration speed of WT, MTM1 KO#1, PI3KC2β KO#1, and double KO#1 undifferentiated myoblasts on a Matrigel matrix. Mean ± SD from three independent experiments represented as fold change compared to control (WT) with a hypothetical mean of 1. For each replicate and condition an average of 40 cells were analyzed. One-way ANOVA ($F = 102.6$) and Dunnett's multiple-comparison test; WT vs. MTM1 KO#1 ****$P < 0.0001$, WT vs. PI3KC2β KO **$P = 0.0039$, WT vs. double KO#1 ns $P = 0.9640$.

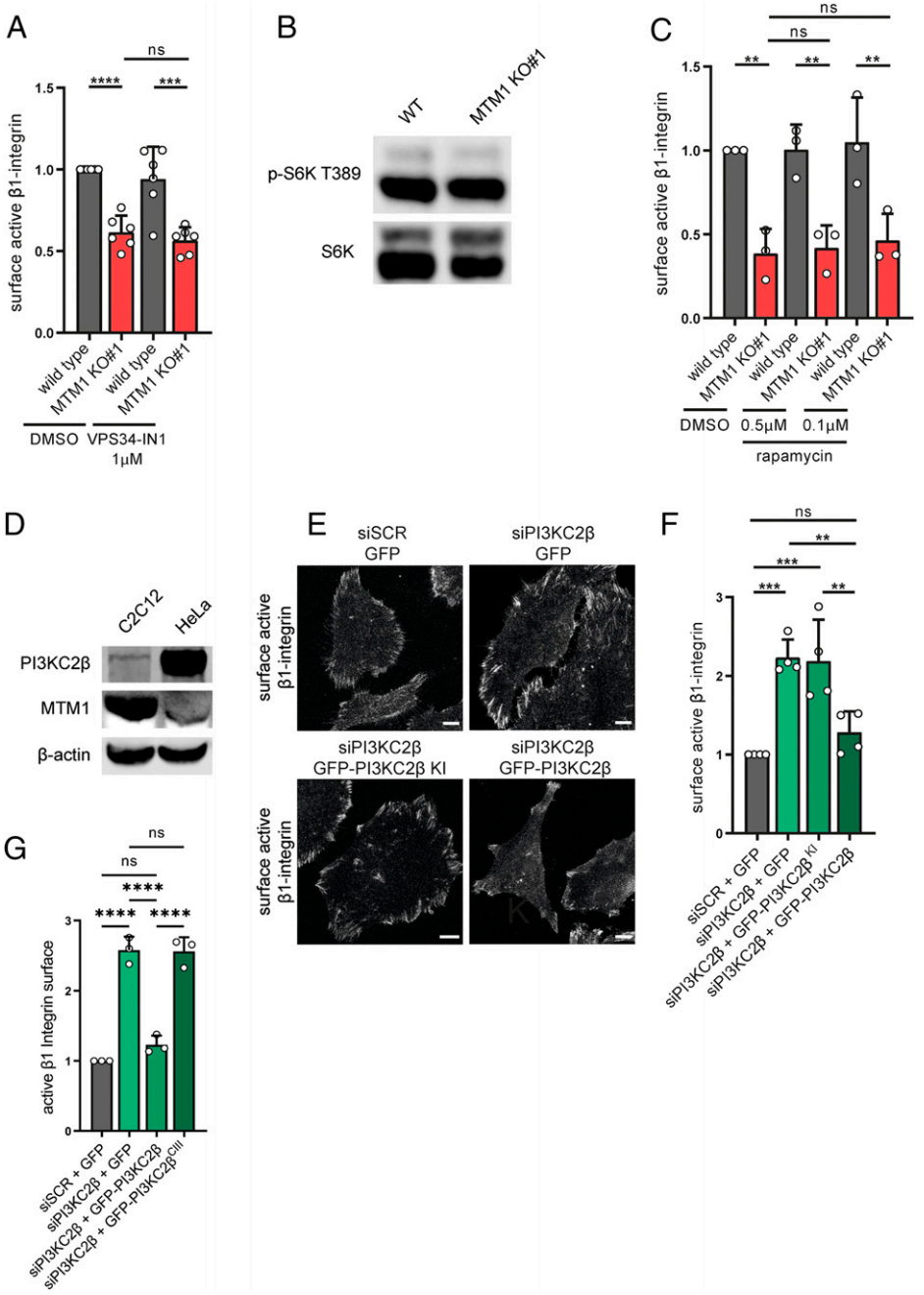

Fig. 3. Rescue of β1-integrin surface pools by loss of active PI3KC2β neither involves mTORC1 nor restoration of cellular PI(3)P levels. (*A*) Surface active β1-integrin intensity per cell in WT and MTM1 KO#1 C2C12 myoblasts treated for 4h with 1 μM VPS34-IN1 or dimethyl sulfoxide (DMSO). Mean ± SD from six independent experiments represented as fold change compared to control (WT+DMSO) with a hypothetical mean of 1. Ten images per condition and experiment were acquired accounting for 50 to 100 cells on average. One-way ANOVA ($F = 21.00$) and Tukey's multiple-comparison test; WT+DMSO vs. MTM1 KO#1+DMSO ****P < 0.0001, WT+VPS34-IN1 vs. MTM1 KO#1+VPS34-IN1 ***P = 0.0001, MTM1 KO#1+DMSO vs. MTM1 KO#1+VPS34-IN1 ns P = 0.8808. (*B*) Immunoblot of p-S6 kinase Thr-389 levels in WT and MTM1 KO#1 C2C12 lysates. (*C*) Surface active β1-integrin intensity per cell in WT and MTM1 KO#1 C2C12 myoblasts treated for 16 h with 0.5 μM or 0.1 μM rapamycin or DMSO. Mean ± SD from three independent experiments represented as fold change compared to control (WT+DMSO) with a hypothetical mean of 1. Ten images per condition and experiment were acquired accounting for 50 to 100 cells on average. One-way ANOVA ($F = 12.224$) and Tukey's multiple-comparison test; WT+DMSO vs. MTM1 KO#1+DMSO **P = 0.0057, WT+0.5 μM vs. MTM1 KO#1 + 0.5 μM **P = 0.0085, WT+0.1 μM vs. MTM1 KO#1 + 0.1 μM **P = 0.0083, MTM1 KO#1+DMSO vs. MTM1 KO#1 + 0.5 μM ns P = 0.9998, MTM1 KO#1+DMSO vs. MTM1 KO#1 + 0.1 μM ns P = 0.9890. (*D*) PI3KC2β protein levels in WT C2C12 and HeLa cells detected by immunoblotting. β-actin is used as a loading control. (*E*) Representative images of HeLa cells treated with control (siSCR) or PI3KC2β-targeting (siPI3KC2β) siRNA and transfected with plasmids encoding for eGFP, eGFP-PI3KC2β, or kinase-inactive eGFP-PI3KC2β (eGFP-PI3KC2β KI) prior to immunostaining for active β1-integrin under nonpermeabilizing conditions. (Scale bar, 10 μm.) (*F*) Surface active β1-integrin intensity per cell in HeLa cells treated with control (siSCR) or PI3KC2β-targeting (siPI3KC2β) siRNA and transfected with plasmids encoding for eGFP, eGFP-PI3KC2β, or kinase-inactive eGFP-PI3KC2β (eGFP-PI3KC2β KI) prior to immunostaining. Mean ± SD from four independent experiments represented as fold change compared to control (siSCR+GFP) with a hypothetical mean of 1. Ten images per condition and experiment were acquired accounting for 30 to 60 cells. One-way ANOVA ($F = 15.83$) and Tukey's multiple-comparison test; siSCR+GFP vs. siPI3KC2β+GFP ***P= 0.0007, siSCR+GFP vs. siPI3KC2β+GFP-PI3KC2β KI ***P = 0.0009, siSCR+GFP vs. siPI3KC2β+GFP-PI3KC2β ns P = 0.6, siPI3KC2β+GFP vs. siPI3KC2β+GFP-PI3KC2β **P = 0.0053, siPI3KC2β+GFP-PI3KC2β KI vs. siPI3KC2β+GFP-PI3KC2β **P = 0.0075. (*G*) Surface active β1-integrin intensity per cell in HeLa cells treated with control (siSCR) or PI3KC2β-targeting (siPI3KC2β) siRNA and transfected with plasmids encoding for eGFP, eGFP-PI3KC2β, or class III like eGFP-PI3KC2β (eGFP-PI3KC2β^{CIII}) prior to immunostaining. Mean ± SD from three independent experiments represented as fold change compared to control (siSCR+GFP) with a hypothetical mean of 1. Ten images per condition and experiment were acquired accounting for 30 to 60 cells. One-way ANOVA ($F = 90.54$) and Tukey's multiple-comparison test; siSCR+GFP vs. siPI3KC2β+GFP ****P< 0.0001, siSCR+GFP vs. siPI3KC2β+GFP-PI3KC2β ns P = 0.3224, siPI3KC2β+GFP vs. siPI3KC2β+GFP-PI3KC2β ****P < 0.0001, siPI3KC2β+GFP vs. siPI3KC2β+GFP-PI3KC2β^{CIII} ns P = 0.9986, siPI3KC2β+GFP-PI3KC2β vs. siPI3KC2β+GFP-PI3KC2β^{CIII} ****P < 0.0001.

mutational analysis (Fig. 4*D*) showed that complex formation of PI3KC2β with clathrin, intersectin 1, and Dab2 is mediated via molecular determinants within its unstructured amino-terminal domain (see scheme in *SI Appendix*, Fig. S5*B*) that harbors independent binding sites for clathrin (21) and intersectin (45) (*SI Appendix*, Fig. S5*C*). The related PI3KC2α enzyme also bound to clathrin but did not coimmunoprecipitate with either intersectin 1 or the β1-integrin adaptor Dab2 (*SI Appendix*, Fig. S5*D*). Importantly, endocytosis of active β1-integrins in HeLa cells depleted of PI3KC2β, intersectin 1, or Dab2 was greatly reduced (Fig. 4*E*), resulting in increased active β1-integrin surface levels (*SI Appendix*, Fig. S5). Defective active β1-integrin endocytosis was also observed in PI3KC2β KO C2C12 myoblasts (*SI Appendix*, Fig. S5 *F* and *G*). By contrast, loss of PI3KC2β in HeLa cells had minor effects on CME of transferrin (*SI Appendix*, Fig. S5*H*), suggesting that it specifically regulates the internalization of active β1-integrins. Reexpression of WT but not KI mutant PI3KC2β restored normal β1-integrin endocytosis in HeLa cells depleted of the endogenous enzyme (Fig. 4*F*). Importantly, defective

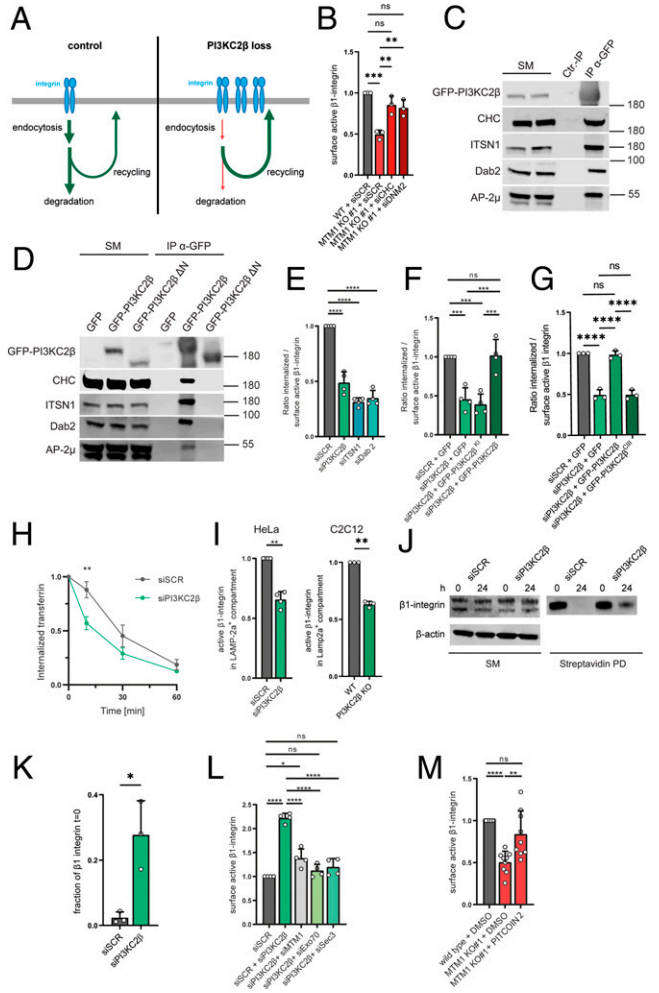

Fig. 4. PI3KC2β and MTM1 antagonistically control active β1-integrin endocytosis and recycling. (*A*) Schematic representation of integrin cycling in control and upon PI3KC2β loss.(*B*) Surface active β1-integrin intensity in WT and MTM1 KO#1 C2C12 myoblasts treated with control (siSCR), clathrin heavy chain- (siCHC), or dynamin2-targeting (siDNM2) siRNA. Mean ± SD from three independent experiments normalized to control (WT + siSCR). 10 images /condition and experiment (30-60 cells) were acquired accounting for . One-way ANOVA ($F = 18.24$) and Tukey's multiple-comparison test; WT + siSCR vs. MTM1 KO#1 + siSCR ***$P = 0.0002$; WT + siSCR vs. MTM1 KO#1 + siCHC ns $P = 0.2946$; WT + siSCR vs. MTM1 KO#1 + siDNM2 ns $P = 0.1408$; MTM1 KO#1 + siSCR vs. MTM1 KO#1 + siCHC **$P = 0.0031$; MTM1 KO#1 + siSCR vs. MTM1 KO#1 + siDNM2 **$P = 0.0282$. (*C*) Immunoprecipitation of eGFP-PI3KC2β from HEK293T cells endogenously expressing eGFP-PI3KC2β. Proteins were detected by immunoblotting from starting material (SM, 5% of total lysate) or bound to GFP-nanotrap magnetic beads (IP α-GFP) or control magnetic beads (Ctr.-IP). (*D*) Immunoprecipitation analysis of proteins associated with eGFP, eGFP-PI3KC2β, or eGFP-PI3KC2β ΔN in HEK293T cells. Samples were analyzed by immunoblotting for clathrin heavy chain (CHC), intersectin 1 (ITSN-1), Dab2, or AP2(μ). SM, 1.25% of total lysate . IP α-GFP, material affinity-captured using GFP-nanotrap magnetic beads. (*E*) Relative internalized to surface active β1-integrin ratio in HeLa cells treated with control (siSCR), PI3KC2β- (siPI3KC2β), ITSN1- (siITSN1), or Dab2-targeting (siDab2) siRNA.Mean ± SD from four independent experiments normalized to control (siSCR). 10 images per condition and experiment (30-60 cells) were acquired . One-way ANOVA ($F = 99.74$) and Tukey's multiple-comparison test; ****$P < 0.0001$. (*F*) Relative internalized to surface active β1-integrin ratio in HeLa cells treated with control (siSCR) or PI3KC2β-targeting (siPI3KC2β) siRNA and transfected with plasmids encoding for eGFP, eGFP-PI3KC2β, or kinase-inactive eGFP-PI3KC2β (eGFP-PI3KC2β KI) prior to immunostaining. Mean ± SD from 4 independent experiments normalized to control (siSCR+GFP). 10 images / condition and experiment (30-60 cells). . One-way ANOVA ($F = 22.52$) and Tukey's multiple-comparison test; siSCR+GFP vs. siPI3KC2β+GFP ***$P = 0.0008$, siSCR+GFP vs. siPI3KC2β+GFP-PI3KC2β KI ***$P = 0.0003$, siSCR+GFP vs. siPI3KC2β+GFP-PI3KC2β ns $P = 0.9981$, siPI3KC2β+GFP vs. siPI3KC2β+GFP-PI3KC2β ***$P = 0.0006$, siPI3KC2β+GFP-PI3KC2β KI vs. siPI3KC2β+GFP-PI3KC2β ***$P = 0.0002$. (*G*) Relative internalized to surface active β1-integrin ratio in HeLa cells treated with control (siSCR) or PI3KC2β-targeting (siPI3KC2β) siRNA and transfected with plasmids encoding for eGFP, eGFP-PI3KC2β, or classIII like eGFP-PI3KC2β (eGFP-PI3KC2β^{CIII}) prior to immunostaining. Mean ± SD from four independent experiments normalized to control (siSCR+GFP) with a hypothetical mean of 1. 10 images / condition and experiment (30-60 cells) were acquired . One-way ANOVA ($F = 104.0$) and Tukey's multiple-comparison test; siSCR+GFP vs. siPI3KC2β+GFP ****$P < 0.0001$, siSCR+GFP vs. siPI3KC2β+GFP-PI3KC2β ns $P = 0.9520$, siPI3KC2β+GFP vs. siPI3KC2β+GFP-PI3KC2βC^{III} ns $P > 0.9999$, siPI3KC2β+GFP vs. siPI3KC2β+GFP-PI3KC2β ****$P < 0.0001$, siPI3KC2β+GFP-PI3KC2β vs. siPI3KC2β+GFP-PI3KC2β^{CIII} ****$P < 0.0001$. (*H*) Transferrin recycling assay in HeLa cells treated with control (siSCR) or PI3KC2β-targeting (siPI3KC2β) siRNA. Internal transferrin pools were quantified after 0, 10, 30, and 60 min. Data normalized to the internal pool at 0 min. Mean ± SEM from 3 independent experiments. 10 images per condition and experiment (30-60 cells) were acquired . One-way ANOVA ($F = 41.48$) and Šídák's multiple comparisons test; siSCR 10 min vs. siPI3KC2β 10 min **$P = 0.0019$, siSCR 30 min vs. siPI3KC2β 30 min ns $P = 0.1433$, siSCR 60 min vs. siPI3KC2β 60 min ns $P = 0.8202$. (*I*) Fraction of active β1-integrin in late endosomal/lysosomal compartment (LAMP-2a) in control (siSCR) and PI3KC2β-depleted (siPI3KC2β) HeLa cells and in undifferentiated WT or PI3KC2β KO C2C12 myoblasts after 4 h of active β1-integrin uptake. Mean ± SD from four independent experiments (HeLa) or three independent experiments (C2C12), respectively. Data normalized to control (siSCR). 10 images per condition and experiment (30-60 cells) were acquired . One-sample two-tailed *t* test; HeLa: **$P = 0.0020$; C2C12: **$P = 0.0019$. (*J*) Streptavidin pulldown using lysates of surface biotinylated HeLa cells treated with control (siSCR) or PI3KC2β targeting (siPI3KC2β) siRNA. Cells were incubated for 0 or 24 h after surface biotinylation, lysed, and remaining surface β1-integrin was analyzed by immunoblotting. (*K*) Quantification of *J*. The ratio of β1-integrin after 24 h and β1-integrin after 0 h is depicted. Mean ± SD from three independent experiments. Two-tailed *t* test; *$P = 0.0141$. (*L*) Surface active β1-integrin intensity per cell in HeLa cells treated with control (siSCR), PI3KC2β- (siPI3KC2β), MTM1- (siMTM1), Exo70- (siExo70), or Sec3-targeting (siSec3) siRNA in the indicated combinations. Mean ± SD from four independent experiments normalized to control (siSCR). One-way ANOVA ($F = 49.88$) and Tukey's multiple-comparison test; siSCR vs. siSCR+siPI3KC2β ****$P < 0.0001$, siSCR vs. siPI3KC2β+siMTM1 *$P = 0.0107$, siSCR vs. siPI3KC2β+siExo70 ns $P = 0.7205$, siSCR vs. siPI3KC2β+siSec3 ns $P = 0.3015$, siSCR+siPI3KC2β vs. siPI3KC2β+siMTM1 ****$P < 0.0001$, siSCR+siPI3KC2β vs. siPI3KC2β+siExo70 ****$P < 0.0001$, siSCR+siPI3KC2β vs. siPI3KC2β+siSec3 ****$P < 0.0001$. (*M*) Surface active β1-integrin intensity in WT and MTM1 KO#1 C2C12 myoblasts treated for 16 h with PITCOIN2 inhibitor or DMSO. Mean ± SD from nine independent experiments normalizedto control (WT+DMSO). 10 images / condition per experiment (50 to 100 cells) were analyzed. One-way ANOVA ($F = 18.43$) and Tukey's multiple-comparison test; WT+DMSO vs. MTM1 KO#1+DMSO ****$P < 0.0001$, WT+DMSO vs. MTM1 KO#1+PITCOIN3 ns $P = 0.1523$, MTM1 KO#1+DMSO vs. MTM1 KO#1+PITCOIN3 **$P = 0.0014$.

β1-integrin endocytosis was not restored upon reexpression of mutant class III-like PI3KC2β lacking the ability to synthesize $PI(3,4)P_2$ (Fig. 4*G*). These results indicate that endocytic clearance of active β1-integrins from the cell surface depends on the ability of PI3KC2β to synthesize $PI(3,4)P_2$. Based on these collective data we hypothesize that clathrin, intersectin 1, and the intersectin-associated integrin adaptor Dab2 may synergize to form an endocytic hub for active β1-integrin internalization.

We noted that the cell-surface levels of active β1-integrins in cells depleted of PI3KC2β appeared to exceed even those induced by loss of the integrin adaptor Dab2 (*SI Appendix*, Fig. S5*E*). Based on these data and previous reports suggesting that PI3KC2β can be recruited to early (17) and late endosomes where it promotes the degradative turnover of autophagy/lysosomal cargoes (19), we hypothesized that PI3KC2β may also impact the downstream endosomal sorting (i.e., recycling vs. lysosomal degradation) of internalized active integrins (Fig. 4*A*). We probed a putative role of PI3KC2β in endosomal sorting at several levels. We found that loss of PI3KC2β resulted in facilitated endosomal recycling of internalized transferrin from endosomes (Fig. 4*H*). Conversely, degradative endosomal sorting of internalized active β1-integrins to LAMP2a-containing lysosomes was perturbed in PI3KC2β KO myoblasts or PI3KC2β-depleted HeLa cells (Fig. 4*I* and *SI Appendix*, Fig. S5*I*). Moreover, while endogenous β1-integrins were effectively cleared from the cell surface of control HeLa cells within 24 h, we observed

a substantial retention of β1-integrins at the plasma membrane of HeLa cells depleted of PI3KC2β (Fig. 4 *J* and *K*). These results suggest that PI3KC2β promotes the internalization and degradative sorting of β1-integrins. Recycling of internalized membrane proteins from endosomes to the plasma membrane depends on active MTM1 and on the hetero-octameric exocyst complex with which MTM1 indirectly associates (5). To assess the possible contribution of elevated endosomal recycling of β1-integrins to the surface of PI3KC2β-depleted cells, we conducted double-knockdown experiments targeting MTM1, or subunits of exocyst, i.e., Exo70 and Sec3. Strikingly, we found that concomitant loss of either MTM1 or the exocyst components Exo70 or Sec3 greatly reduced the surface accumulation of active β1-integrins in HeLa cells depleted of PI3KC2β (Fig. 4*L*).

These collective findings show that PI3KC2β and MTM1 antagonistically control active β1-integrin endocytosis and recycling to the cell surface from endosomes. Hence, specific pharmacological inhibition of PI3KC2β catalysis would be predicted to restore active β1-integrin surface pools caused by loss of MTM1 function. No specific membrane-permeant pharmacological inhibitors of class II PI3Ks including PI3KC2β have been available so far. We recently combined high-throughput screening with medicinal chemistry approaches to identify tool compounds that selectively inhibit the activity of PI3KC2α (48). One of the identified compounds, termed PITCOIN2, displayed off-target activity toward PI3KC2β with a concentration that inhibits response by 50% (IC_{50}) of 1.5 μM, while leaving other lipid kinases including VPS34 and class I PI3Ks unperturbed (*SI Appendix*, Fig. S6*A*) (48). Pharmacological inhibition of PI3KC2β function in the presence of PITCOIN2 indeed potently elevated the surface levels of active β1-integrins in HeLa cells, essentially phenocopying genetic loss of PI3KC2β (*SI Appendix*, Fig. S6 *B* and *C*). In contrast, when HeLa cells were treated with the PI3KC2α-selective inhibitor PITCOIN3 the surface levels of active β1-integrins remained unaltered (*SI Appendix*, Fig. S6 *B* and *C*). Moreover, application of PITCOIN2 partially restored the surface levels of active β1-integrins in MTM1 KO myoblasts (Fig. 4*I* and *SI Appendix*, Fig. S6*D*). The potent inhibitory effect on PI3KC2α, an essential gene in mice (18), prevented us from exploring the effects of long-term (more than many days) application of PITCOIN2 on MTM1 KO myoblasts further. Nonetheless, our data provide proof of principle that isoform-selective pharmacological inhibition of PI3KC2β activity may be a viable option to rescue XLCNM phenotypes in cell- and animal-based models and, possibly, in patients.

Discussion

In this study we identify the lipid kinase PI3KC2β as a genetic and functional modifier of MTM1 function in a cell-based model of XLCNM. We demonstrate that genetic KO of *Pik3c2b* or pharmacological inhibition of PI3KC2β activity rescues reduced active β1-integrin surface levels and other key phenotypes of MTM1 dysfunction such as defective myoblast differentiation and reduced numbers of FAs that underlie XLCNM pathology. Surprisingly, however, loss of PI3KC2β does not appear to act by restoring endosomal PI(3)P levels increased following absence of MTM1, distinct from earlier suggestions (14, 15). We further show that PI3KC2β acts by facilitating the endocytosis and degradative endosomal sorting of active β1-integrins, thereby controlling their plasma membrane levels in myoblasts and nonmuscle cells. Together with previous studies (5, 10) that have established a role for MTM1 in the delivery of β-integrins to the cell surface, our findings suggest a model whereby PI3KC2β and MTM1 antagonistically control active β1-integrin endocytosis and recycling to the plasma membrane from endosomes, while acting on different pools of PI 3-phosphates. A key role for β1-integrin endocytosis and recycling in centronuclear myopathy is underscored by the fact that gain-of-function mutations in the endocytic protein dynamin 2 that lead to elevated dynamin 2 protein levels cause an autosomal dominant form of the disease (49). Conversely, genetic depletion of dynamin 2 (33, 44, 50) or post-transcriptional reduction of dynamin 2 protein expression induced by tamoxifen (51) improved phenotypes of MTM1 loss in a murine model of XLCNM, although the relationship to β1-integrins had not been explored in these studies. Whether loss or inhibition of PI3KC2β also rescues other XLCNM phenotypes, e.g., defects in nuclei positioning or the organization of the sarcoplasmic reticulum (25), will need to be addressed in the future.

Given that PI3KC2β loss leads to selective defects in the endocytosis of active β1-integrins but is largely dispensable for CME of transferrin, we favor a model whereby PI3KC2β via association with intersectin 1 (45) and the associated integrin adaptor Dab2 (47) serves a cargo-selective function in targeting active β1-integrins to sites of endocytic vesicle formation. Previous work has identified multiple pathways (52) that differentially contribute to the endocytosis and recycling of active and inactive β-integrins (29) including clathrin-based mechanisms (47, 53, 54), the CLIC/GEEC pathway (55), and the surface delivery of matrix metalloproteases from lysosomes to cleave active β-integrins from the extracellular fibronectin matrix (56). PI3KC2β may conceivably regulate several of these processes. In addition to its endocytic function at plasma membrane clathrin-coated pits (this study) it might, for example, contribute to the surface delivery of matrix metalloproteases from lysosomes to which PI3KC2β has been localized (19, 20). Internalized active β-integrins are either retained intracellularly, recycled to the cell surface (52), a pathway mediated by MTM1 and the exocyst complex (5), or sorted to lysosomes for proteolytic turnover. Our data favor a mechanism in which the decision to recycle, retain, or degrade β1-integrins is controlled by active PI3KC2β, likely at the level of endosomes or primary endocytic vesicles (17). The precise mechanism by which active PI3KC2β facilitates degradative sorting of internalized active β1-integrins will need to await future studies. For example, local PI3KC2β-mediated synthesis of PI 3-phosphates may serve to selectively recruit lipid-binding endosomal effector proteins such as ESCRT proteins as recently demonstrated for the related PI3KC2α isoform in the context of cytokinesis (57).

Irrespective of the precise mechanism of β1-integrin sorting our study provides prima facie evidence that acute pharmacological inhibition of PI3KC2β activity can rescue key features of MTM1 deficiency and may therefore provide a therapeutic option for XLCNM patients. The development of the class II PI 3-kinase inhibitor PITCOIN2 may serve as a starting point for the future development of small molecules that selectively interfere with PI3KC2β function at the organismic level, albeit possible concerns remain with respect to adverse effects of PI3KC2β inhibitors in nonmuscle tissue. The tools developed here will serve to pave the way toward this goal.

Materials and Methods

Antibodies. See *SI Appendix*, Table S1.

Plasmids. Complementary DNA encoding human MTM1 was inserted into mCherry-pcDNA3.1(+), resulting in expression of an N-terminally mCherry-tagged protein, as described before (5). An MTM1 phosphatase-inactive mutant mCherry-MTM1^{C375S} was also generated and described in the same publication. FL eGFP-PI3KC2β, KI eGFP-PI3KC2β, and eGFP-PI3KC2β ΔN were described

previously (13, 14). eGFP-PI3KC2α was described previously (29). eGFP-PI3KC2βC^{III} was described before (11).

Cell Lines. Cos7, HEK293T, HeLa, and C2C12 were obtained from ATCC and not used beyond passage 30 from original derivation by ATCC. HEK293T and HeLa cells expressing endogenous eGFP-PI3KC2β were described previously (13, 14). Cell lines were routinely tested for mycoplasma contamination.

C2C12 Cell Culture and Differentiation. Myoblastic cell line C2C12 (ATCC CRL-1772) was cultured in growth media (GM) containing Dulbecco's modified Eagle's medium (DMEM) with 25 mM D-glucose, 4 mM L-glutamine, and phenol red (Gibco) supplemented with 10% (vol/vol) heat-inactivated fetal bovine serum (FBS; Gibco), 100 U/mL penicillin, and 100 μg/mL streptomycin (Gibco). Cells were routinely maintained at low confluency (<70%) and seeded for experiments at low passage number. For immunocytochemistry, cells were seeded on Matrigel (Corning)-coated glass coverslips, whereas no coating was used for protein extraction experiments.

For C2C12 differentiation, either 4×10^4 cells per well were seeded on 0.1% (wt/vol) gelatin (Sigma)-coated ibiTreat eight-well chambers (ibidi) or 3×10^5 cells were seeded on 0.1% (wt/vol) gelatin-coated six-well plates. On the following day (differentiation day 0), cells were confluent and GM was replaced by differentiation media (DM), containing DMEM with 25 mM D-glucose, 4 mM L-glutamine, and phenol red (Gibco) supplemented with 2% (vol/vol) horse serum (Gibco), 100 U/mL penicillin, and 100 μg/mL streptomycin (Gibco). From the following day on, DM was exchanged every 24 h. Cells were processed on day 7.

HeLa Cell Culture. The HeLa cell line was cultured in cell culture media containing DMEM with 25 mM D-glucose, 4 mM L-glutamine, and phenol red (Gibco) supplemented with 10% (vol/vol) heat-inactivated FBS (Gibco), 100 U/mL penicillin, and 100 μg/mL streptomycin (Gibco). Cells were not used beyond passage 30.

Generation of CRISPR-Cas–Engineered C2C12 Cell Lines. For generation of MTM1, PI3KC2β and double-KO C2C12 cell lines single-guide RNA (sgRNA) was cloned into Cas9 (*Streptococcus pyogenes*) green fluorescent protein (GFP) plasmid px458-pSpCas9(BB)-2A-GFP (Addgene, #48138). C2C12 cells at passage 3 were transfected with px458 plasmid containing *Mtm1*- and *Pik3c2b*-targeting sgRNA inserts using jetPRIME (Polyplus). GFP-expressing cells were sorted into 96-well plates using fluorescence-activated single cell sorter (BD FACSAria). Colonies were expanded and screened for genetic alterations at the sgRNA target site via sequencing and insertion-deletion (InDel) estimation and, subsequently, by immunoblotting. See *SI Appendix, Extended Methods* for further details.

Flow Cytometry. For flow cytometric analysis, cultured C2C12 cells were rinsed with Dulbecco's phosphate-buffered saline (DPBS; Gibco) and detached with a 5-min incubation with Pronase (Sigma-Aldrich) at room temperature. Cells were collected in tubes and washed by adding DPBS containing 2% FBS and spinning down for 3 min at 500 rpm. Pelleted cells were resuspended in 5% bovine serum albumin (BSA) in PBS and incubated with primary antibodies for 60 min at 4 °C. Subsequently, cells were washed three times in ice-cold PBS and stained with secondary antibodies in PBS + 5% BSA for 45 min at 4 °C. After three washes in PBS cells were analyzed using a BD LSR Fortessa flow cytometer.

Statistics and Reproducibility. Values are depicted as mean ± SD. One-sample two-sided *t* tests were used for comparisons with control group values that had been set to 1 for normalization purposes and that therefore did not fulfill the requirement of two-sample *t* tests. One-way ANOVA with Dunnet's or Tukey's multiple-comparison tests were used to compare three or more groups after the same normalization. GraphPad Prism version 9 software was used for statistical analysis. The level of significance is indicated in the figures by asterisks ($*P < 0.05$; $**P < 0.01$; $***P < 0.001$; $****P < 0.0001$) and provided in the figure legends as exact *P* value obtained by the indicated statistical test. No statistical method was used to predetermine sample size as sample sizes were not chosen based on prespecified effect size. Instead, multiple independent experiments were carried out using several sample replicates as detailed in the figure legends.

Extended Methods. *SI Appendix, Extended Methods* contain information on oligonucleotides and siRNAs; generation of CRISPR-Cas9–engineered C2C12 cell lines; transfection of cultured cells; lentiviral transduction of C2C12 cells; chemicals and inhibitors; cell lysates, immunocytochemistry; microscopy and image analysis, cell migration; detection of PI(3)P, integrin uptake assay; transferrin uptake, surface labeling, and recycling; surface biotinylation and determination of surface β1-integrin turnover; GST pulldown assays; and immunoprecipitations.

Data, Materials, and Software Availability. All study data are included in the article and/or *SI Appendix*.

ACKNOWLEDGMENTS. We thank Dr. Alexander Wallroth for help with initial experiments regarding the cell-surface levels of active β1-integrins and Claudia Schmidt, Maria Mühlbauer, Delia Löwe, and Silke Zillmann for expert technical assistance. Supported by the Deutsche Forschungsgemeinschaft (HA2686/15-1 [E-RARE: Treat MTMs] to V.H.). P.S. was supported by the European Union as part of the H2020-funded ITN "Phd" (grant agreement 675392).

1. M. W. Lawlor, J. J. Dowling, X-linked myotubular myopathy. *Neuromuscul. Disord.* **31**, 1004–1012 (2021).
2. J. Laporte *et al.*, A gene mutated in X-linked myotubular myopathy defines a new putative tyrosine phosphatase family conserved in yeast. *Nat. Genet.* **13**, 175–182 (1996).
3. Y. Posor, W. Jang, V. Haucke, Phosphoinositides as membrane organizers. *Nat. Rev. Mol. Cell Biol.*, 10.1038/s41580-022-00490-x (2022).
4. F. Blondeau *et al.*, Myotubularin, a phosphatase deficient in myotubular myopathy, acts on phosphatidylinositol 3-kinase and phosphatidylinositol 3-phosphate pathway. *Hum. Mol. Genet.* **9**, 2223–2229 (2000).
5. K. Ketel *et al.*, A phosphoinositide conversion mechanism for exit from endosomes. *Nature* **529**, 408–412 (2016).
6. J. Laporte, F. Bedez, A. Bolino, J. L. Mandel, Myotubularins, a large disease-associated family of cooperating catalytically active and inactive phosphoinositides phosphatases. *Hum. Mol. Genet.* **12**, R285–R292 (2003).
7. M. A. Raess, S. Friant, B. S. Cowling, J. Laporte, WANTED - Dead or alive: Myotubularins, a large disease-associated protein family. *Adv. Biol. Regul.* **63**, 49–58 (2017).
8. G. S. Taylor, T. Maehama, J. E. Dixon, Myotubularin, a protein tyrosine phosphatase mutated in myotubular myopathy, dephosphorylates the lipid second messenger, phosphatidylinositol 3-phosphate. *Proc. Natl. Acad. Sci. U.S.A.* **97**, 8910–8915 (2000).
9. V. M. Lionello *et al.*, Amphiphysin 2 modulation rescues myotubular myopathy and prevents focal adhesion defects in mice. *Sci. Transl. Med.* **11**, eaav1866 (2019).
10. I. Ribeiro, L. Yuan, G. Tanentzapf, J. J. Dowling, A. Kiger, Phosphoinositide regulation of integrin trafficking required for muscle attachment and maintenance. *PLoS Genet.* **7**, e1001295 (2011).
11. M. Schwander *et al.*, Beta1 integrins regulate myoblast fusion and sarcomere assembly. *Dev. Cell* **4**, 673–685 (2003).
12. Z. Sun, S. S. Guo, R. Fässler, Integrin-mediated mechanotransduction. *J. Cell Biol.* **215**, 445–456 (2016).
13. M. Rozo, L. Li, C. M. Fan, Targeting β1-integrin signaling enhances regeneration in aged and dystrophic muscle in mice. *Nat. Med.* **22**, 889–896 (2016).
14. N. Sabha *et al.*, PIK3C2B inhibition improves function and prolongs survival in myotubular myopathy animal models. *J. Clin. Invest.* **126**, 3613–3625 (2016).
15. M. Velichkova *et al.*, Drosophila Mtm and class II PI3K coregulate a PI(3)P pool with cortical and endolysosomal functions. *J. Cell Biol.* **190**, 407–425 (2010).
16. Y. Posor *et al.*, Local synthesis of the phosphatidylinositol-3,4-bisphosphate lipid drives focal adhesion turnover. *Dev. Cell* **57**, 1694–1711.e7 (2022).
17. S. Alliouachene *et al.*, Inactivation of the class II PI3K-C2β potentiates insulin signaling and sensitivity. *Cell Rep.* **13**, 1881–1894 (2015).
18. F. Gulluni, M. C. De Santis, J. P. Margaria, M. Martini, E. Hirsch, Class II PI3K functions in cell biology and disease. *Trends Cell Biol.* **29**, 339–359 (2019).
19. A. L. Marat *et al.*, mTORC1 activity repression by late endosomal phosphatidylinositol 3,4-bisphosphate. *Science* **356**, 968–972 (2017).
20. A. Wallroth, P. A. Koch, A. L. Marat, E. Krause, V. Haucke, Protein kinase N controls a lysosomal lipid switch to facilitate nutrient signalling via mTORC1. *Nat. Cell Biol.* **21**, 1093–1101 (2019).
21. M. Wheeler, J. Domin, The N-terminus of phosphoinositide 3-kinase-C2beta regulates lipid kinase activity and binding to clathrin. *J. Cell. Physiol.* **206**, 586–593 (2006).
22. M. W. Lawlor *et al.*, Myotubularin-deficient myoblasts display increased apoptosis, delayed proliferation, and poor cell engraftment. *Am. J. Pathol.* **181**, 961–968 (2012).
23. C. Gavriilidis *et al.*, The MTM1-UBQLN2-HSP complex mediates degradation of misfolded intermediate filaments in skeletal muscle. *Nat. Cell Biol.* **20**, 198–210 (2018).
24. J. R. Volpatti *et al.*, X-linked myotubular myopathy is associated with epigenetic alterations and is ameliorated by HDAC inhibition. *Acta Neuropathol.* **144**, 537–563 (2022).
25. L. Al-Qusairi *et al.*, T-tubule disorganization and defective excitation-contraction coupling in muscle fibers lacking myotubularin lipid phosphatase. *Proc. Natl. Acad. Sci. U.S.A.* **106**, 18763–18768 (2009).
26. A. Buj-Bello *et al.*, The lipid phosphatase myotubularin is essential for skeletal muscle maintenance but not for myogenesis in mice. *Proc. Natl. Acad. Sci. U.S.A.* **99**, 15060–15065 (2002).
27. B. Geiger, J. P. Spatz, A. D. Bershadsky, Environmental sensing through focal adhesions. *Nat. Rev. Mol. Cell Biol.* **10**, 21–33 (2009).
28. J. Alanko *et al.*, Integrin endosomal signalling suppresses anoikis. *Nat. Cell Biol.* **17**, 1412–1421 (2015).
29. A. Arjonen, J. Alanko, S. Veltel, J. Ivaska, Distinct recycling of active and inactive β1 integrins. *Traffic* **13**, 610–625 (2012).
30. M. Lenter *et al.*, A monoclonal antibody against an activation epitope on mouse integrin chain beta 1 blocks adhesion of lymphocytes to the endothelial integrin alpha 6 beta 1. *Proc. Natl. Acad. Sci. U.S.A.* **90**, 9051–9055 (1993).
31. M. Spiess *et al.*, Active and inactive β1 integrins segregate into distinct nanoclusters in focal adhesions. *J. Cell Biol.* **217**, 1929–1940 (2018).
32. K. Hnia, I. Vaccari, A. Bolino, J. Laporte, Myotubularin phosphoinositide phosphatases: Cellular functions and disease pathophysiology. *Trends Mol. Med.* **18**, 317–327 (2012).

33. H. Tasfaout, B. S. Cowling, J. Laporte, Centronuclear myopathies under attack: A plethora of therapeutic targets. *J. Neuromuscul. Dis.* **5**, 387–406 (2018).
34. G. R. Hammond, G. Schiavo, R. F. Irvine, Immunocytochemical techniques reveal multiple, distinct cellular pools of PtdIns4P and PtdIns(4,5)P(2). *Biochem. J.* **422**, 23–35 (2009).
35. C. Raiborg *et al.*, FYVE and coiled-coil domains determine the specific localisation of Hrs to early endosomes. *J. Cell Sci.* **114**, 2255–2263 (2001).
36. J. J. Dowling *et al.*, Loss of myotubularin function results in T-tubule disorganization in zebrafish and human myotubular myopathy. *PLoS Genet.* **5**, e1000372 (2009).
37. G. Di Paolo, P. De Camilli, Phosphoinositides in cell regulation and membrane dynamics. *Nature* **443**, 651–657 (2006).
38. T. Balla, Phosphoinositides: Tiny lipids with giant impact on cell regulation. *Physiol. Rev.* **93**, 1019–1137 (2013).
39. R. Bago *et al.*, Characterization of VPS34-IN1, a selective inhibitor of Vps34, reveals that the phosphatidylinositol 3-phosphate-binding SGK3 protein kinase is a downstream target of class III phosphoinositide 3-kinase. *Biochem. J.* **463**, 413–427 (2014).
40. H. Tronchère *et al.*, Production of phosphatidylinositol 5-phosphate by the phosphoinositide 3-phosphatase myotubularin in mammalian cells. *J. Biol. Chem.* **279**, 7304–7312 (2004).
41. L. Gozzelino *et al.*, Defective lipid signalling caused by mutations in PIK3C2B underlies focal epilepsy. *Brain* **145**, 2313–2331 (2022).
42. Y. Posor *et al.*, Spatiotemporal control of endocytosis by phosphatidylinositol-3,4-bisphosphate. *Nature* **499**, 233–237 (2013).
43. P. Moreno-Layseca, J. Icha, H. Hamidi, J. Ivaska, Integrin trafficking in cells and tissues. *Nat. Cell Biol.* **21**, 122–132 (2019).
44. B. S. Cowling *et al.*, Reducing dynamin 2 expression rescues X-linked centronuclear myopathy. *J. Clin. Invest.* **124**, 1350–1363 (2014).
45. M. Das *et al.*, Regulation of neuron survival through an intersectin-phosphoinositide 3′-kinase C2beta-AKT pathway. *Mol. Cell. Biol.* **27**, 7906–7917 (2007).
46. A. Pechstein *et al.*, Regulation of synaptic vesicle recycling by complex formation between intersectin 1 and the clathrin adaptor complex AP2. *Proc. Natl. Acad. Sci. U.S.A.* **107**, 4206–4211 (2010).
47. A. Teckchandani, E. E. Mulkearns, T. W. Randolph, N. Toida, J. A. Cooper, The clathrin adaptor Dab2 recruits EH domain scaffold proteins to regulate integrin β1 endocytosis. *Mol. Biol. Cell* **23**, 2905–2916 (2012).
48. W. T. Lo *et al.*, Development of selective inhibitors of phosphatidylinositol 3-kinase C2a. *Nat. Chem. Biol.* https://www.nature.com/articles/s41589-022-01118-z (2022).
49. S. Buono *et al.*, Reducing dynamin 2 (DNM2) rescues *DNM2*-related dominant centronuclear myopathy. *Proc. Natl. Acad. Sci. U.S.A.* **115**, 11066–11071 (2018).
50. H. Tasfaout *et al.*, Antisense oligonucleotide-mediated Dnm2 knockdown prevents and reverts myotubular myopathy in mice. *Nat. Commun.* **8**, 15661 (2017).
51. N. Maani *et al.*, Tamoxifen therapy in a murine model of myotubular myopathy. *Nat. Commun.* **9**, 4849 (2018).
52. G. Mana, D. Valdembri, G. Serini, Conformationally active integrin endocytosis and traffic: Why, where, when and how? *Biochem. Soc. Trans.* **48**, 83–93 (2020).
53. W. T. Chao *et al.*, Type I phosphatidylinositol phosphate kinase beta regulates focal adhesion disassembly by promoting beta1 integrin endocytosis. *Mol. Cell. Biol.* **30**, 4463–4479 (2010).
54. F. Baschieri *et al.*, Frustrated endocytosis controls contractility-independent mechanotransduction at clathrin-coated structures. *Nat. Commun.* **9**, 3825 (2018).
55. P. Moreno-Layseca *et al.*, Cargo-specific recruitment in clathrin- and dynamin-independent endocytosis. *Nat. Cell Biol.* **23**, 1073–1084 (2021).
56. E. Rainero *et al.*, Ligand-occupied integrin internalization links nutrient signaling to invasive migration. *Cell Rep.* **10**, 398–413 (2015).
57. F. Gulluni *et al.*, PI(3,4)P2-mediated cytokinetic abscission prevents early senescence and cataract formation. *Science* **374**, eabk0410 (2021).